Supplementary Figure 1

Three different trap geometries

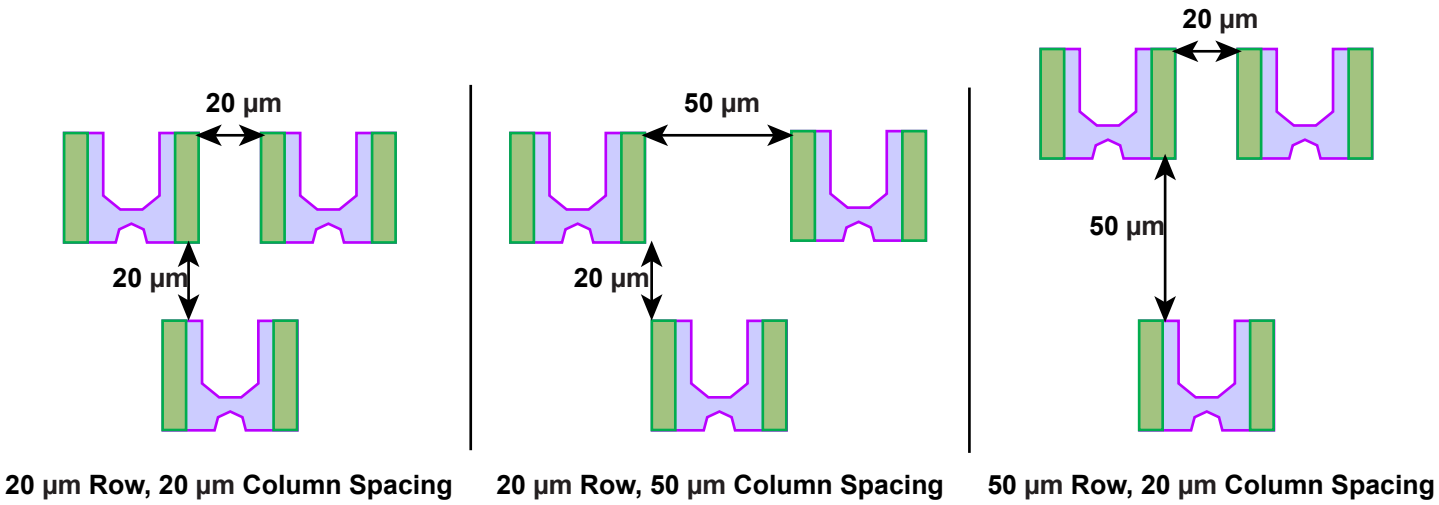

The left-most geometry has equal row and column spacing: the capture efficiency is ~ 90% but the device is prone to clogging. The middle geometry has a 50 µm column spacing and a 20 µm row spacing: the resulting capture efficiency is ~ 5%. The right-most geometry has 20 µm column spacing and 50 µm row spacing: the resulting capture efficiency is ~ 70% and the device is less prone to clogging.

Supplementary Figure 2

Fusion efficiency with multiple doses of PEG

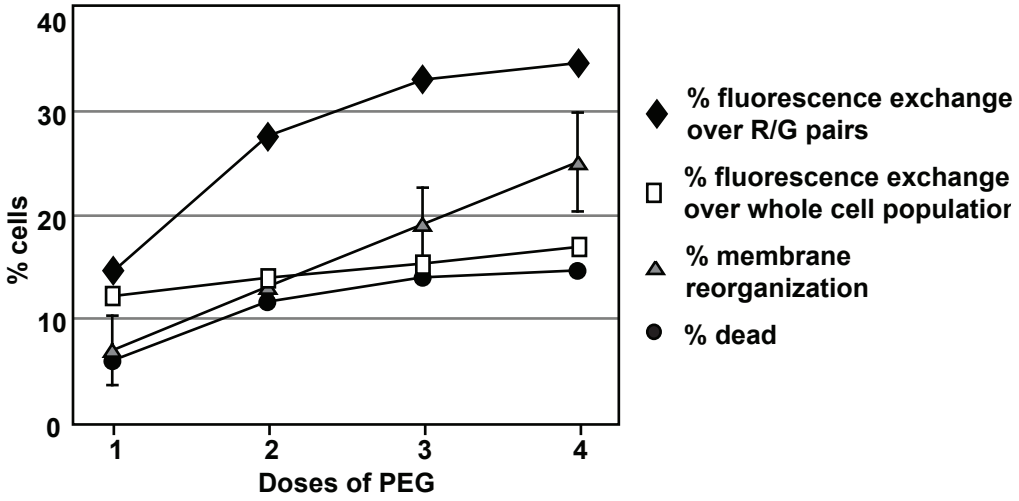

Fusion efficiency with multiple doses of PEG, measured by both fluorescence exchange and membrane reorganization. Each value represents the cumulative total at each dose. Diamond symbols represent fusion efficiency, determined by fluorescence exchange over the correctly paired cells only, while square symbols measure fusion efficiency over the entire array (# of red-green double-positive cells divided by the total number of cells). Membrane reorganization over the entire array is measured in a separate experiment that fused unstained 3T3s with CellTracker-stained 3T3s, while number of dead cells over the entire array were determined after each dose by trypan blue exclusion. With 4 doses of PEG ~ 15% fluorescence exchange is observed (35% over red/green pairs) and ~ 25% membrane reorganization is obtained, with ~15% dead cells.

Supplementary Figure 3

Electrofusion optimization device

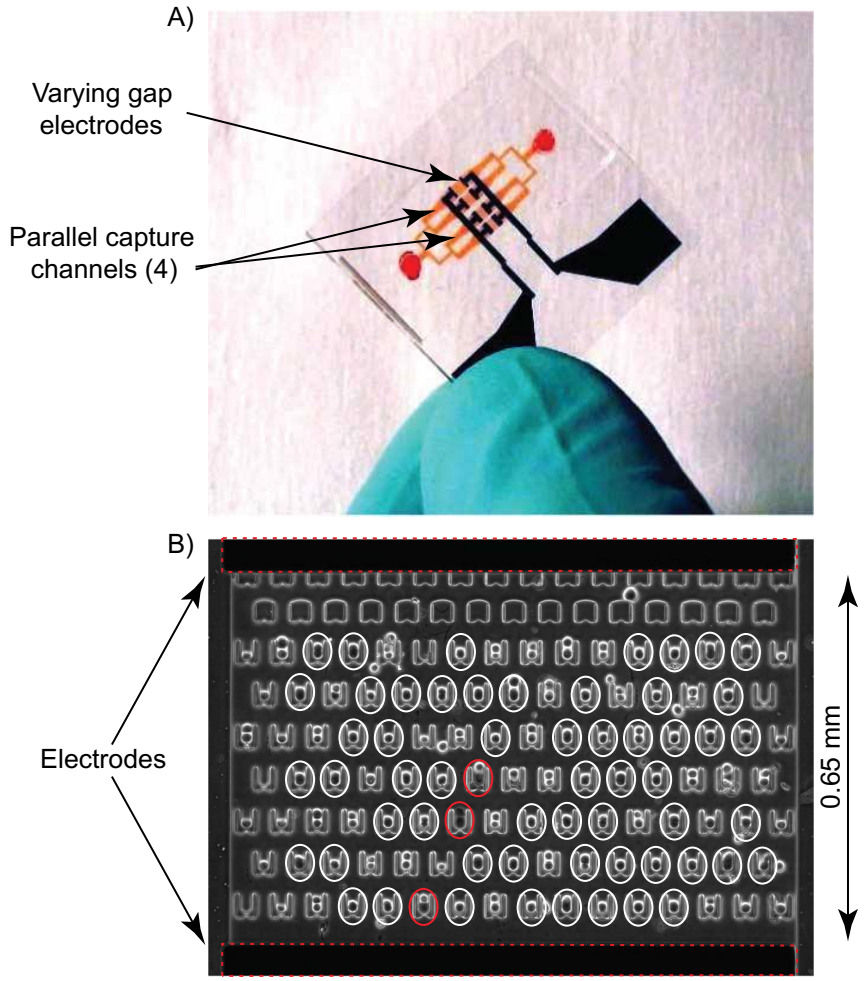

(A) The device contains four independent fusion chambers fed by one inlet, allowing distribution of a single cell population among four test conditions. The electrode gaps vary from chamber to chamber, providing a ~1.7× variation in field strength across the device, while only needing connection to one electrofusion power supply. This provides the ability to test a number of field strengths at once to optimize the fusion parameters. B) Image of cells within a particular chamber (with 0.65-mm electrode gap) following application of an electrofusion pulse. By imaging cells before and after fusion, successful fusions can be observed (white circles). Dead cells can be observed by the loss of bright border in the phase image (red circles), and, if loaded with fluorescent dye, will also leak the dye out over time (not shown).

Supplementary Figure 4

Electrofusion of Celltracker-stained 3T3s

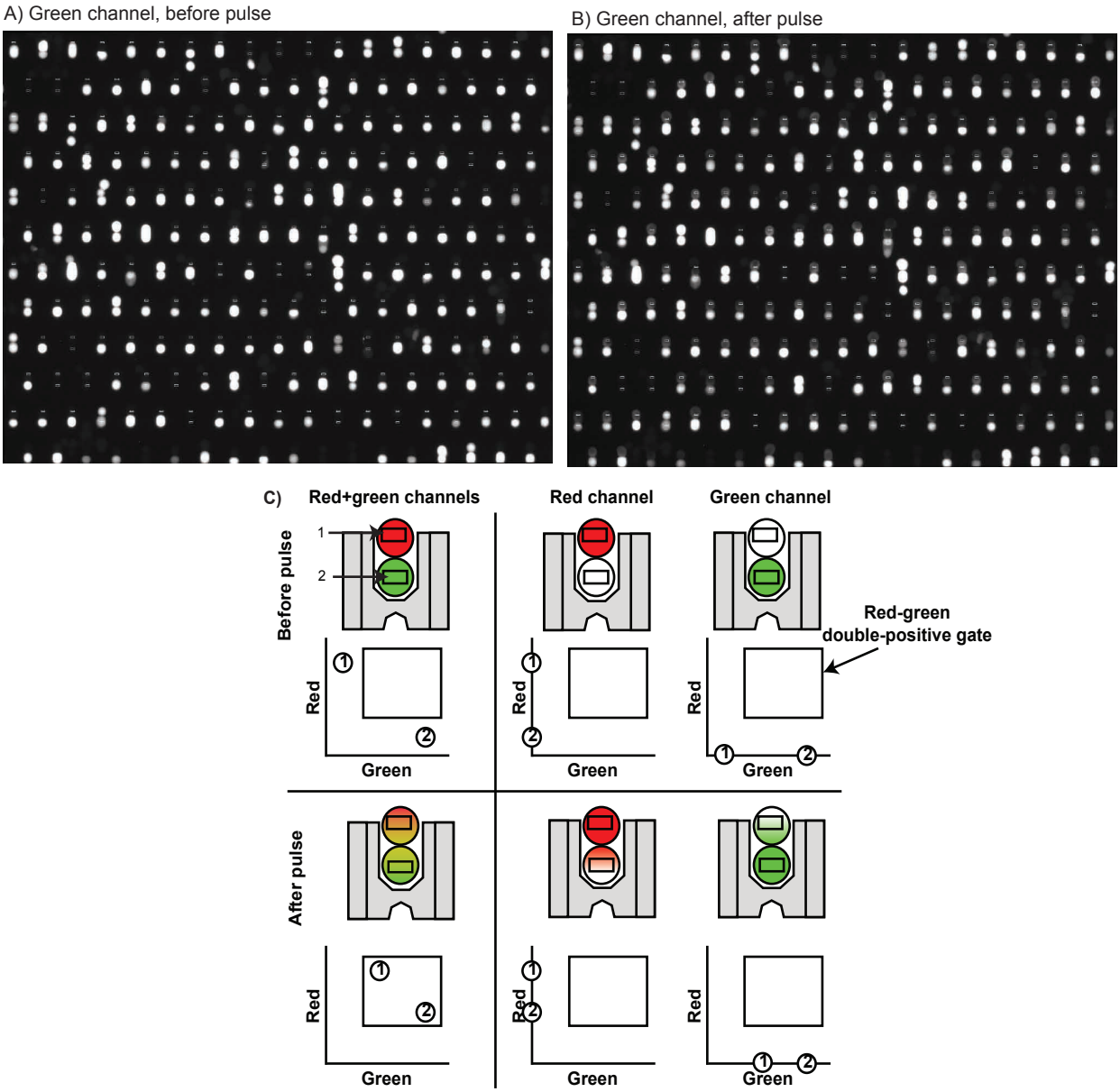

A and B) Raw data for the electrofusion of CellTracker-stained 3T3s. The two images observed are for the green channel, before and immediately after the fusion pulse. The locations of the image analysis rectangles are shown, and these rectangles remain stationary across both the green/red channels and at all time points analyzed. This data corresponds to the plots shown in Figure 4. C) Schematic of the image analysis protocol, and corresponding FACS plot data. The left-most column shows the combination of both channels, while the right columns break down the data into red and green channels. After the fusion pulse the red and green cells pick up fluorescence from the opposite cell, and move inside the red-green double-positive gate. Efficiencies are calculated as the number of red-green double-positive cells over the total number of cells.

Supplementary Figure 5

Analysis of Fusion Efficiencies with FlowJo

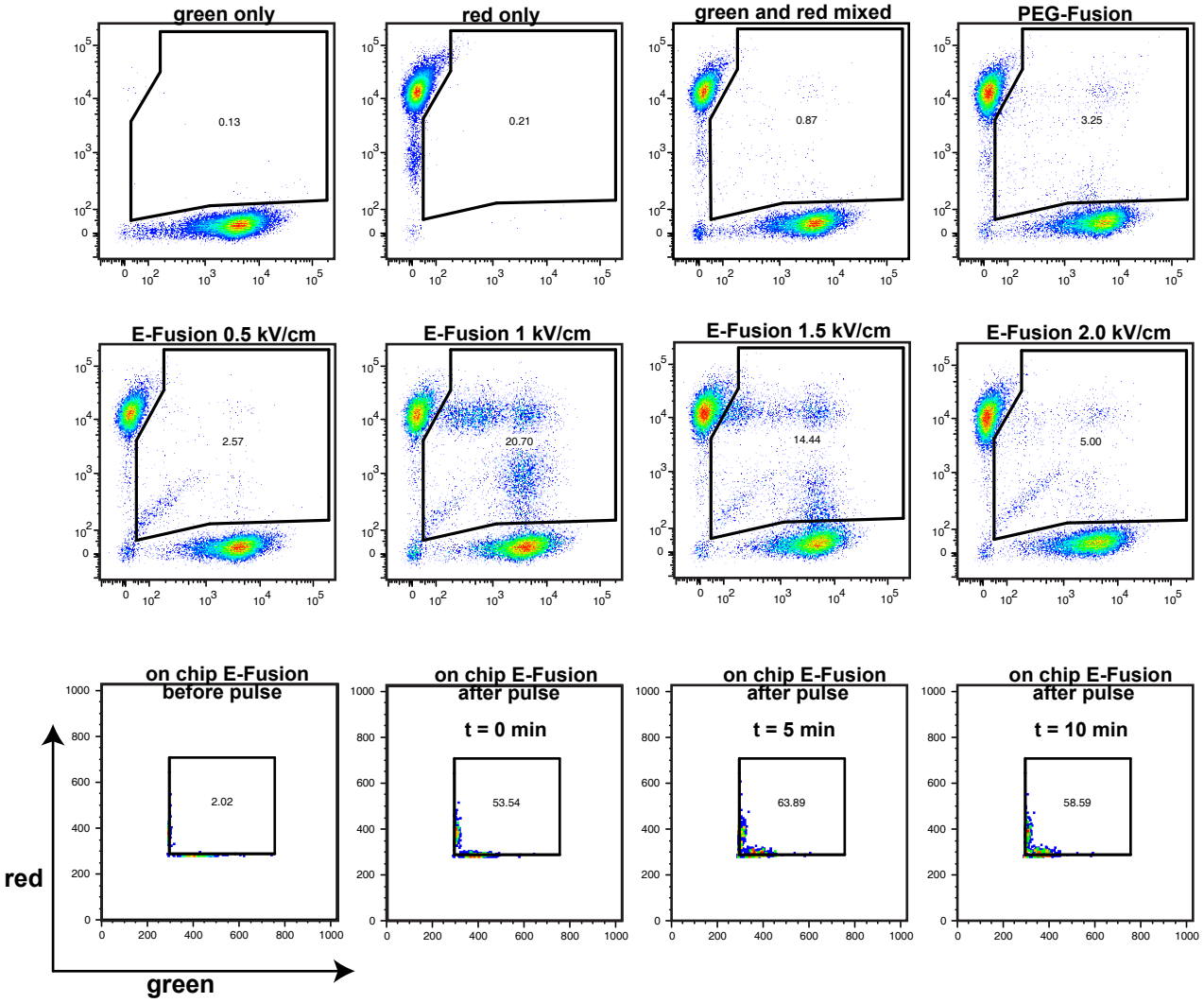

The top row of plots show the control data and location of gates as well as a control PEG run, and the middle row show the voltage optimization for the Eppendorf Helix chamber. The bottom row of plots show the location of gates for cells fused in the microfluidic device. All data shown is included in Figure 4.

Supplementary Figure 6

Analysis of fusion over time

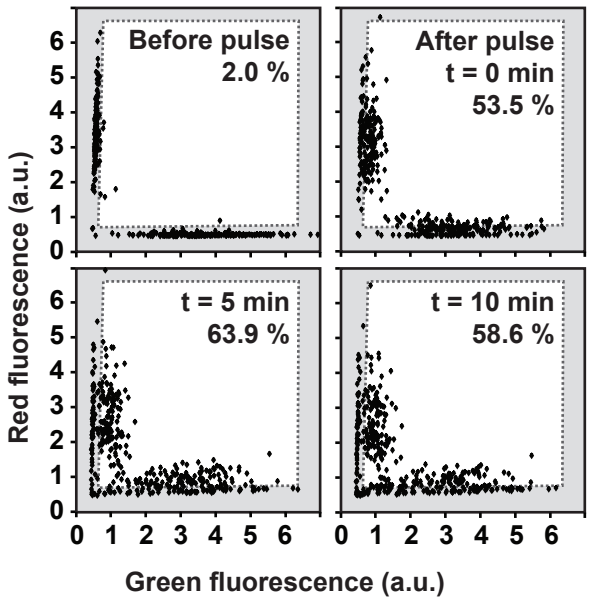

The mean green and red value of a small rectangular area was determined for each of the cells in all of the capture cups in the field of view. Immediately after the fusion pulse fluorescence exchange is observed, indicated by the green population increasing in red intensity and vice versa. The time point before the pulse was used to determine the location of the gates, and these gates (approximate location indicated by white boxes) were applied to the remaining time points. See Supplementary Fig. 4 for raw images and Supplementary Fig. 5 for gate locations.

Supplementary Figure 7

Culture in absence of fusion stimulus

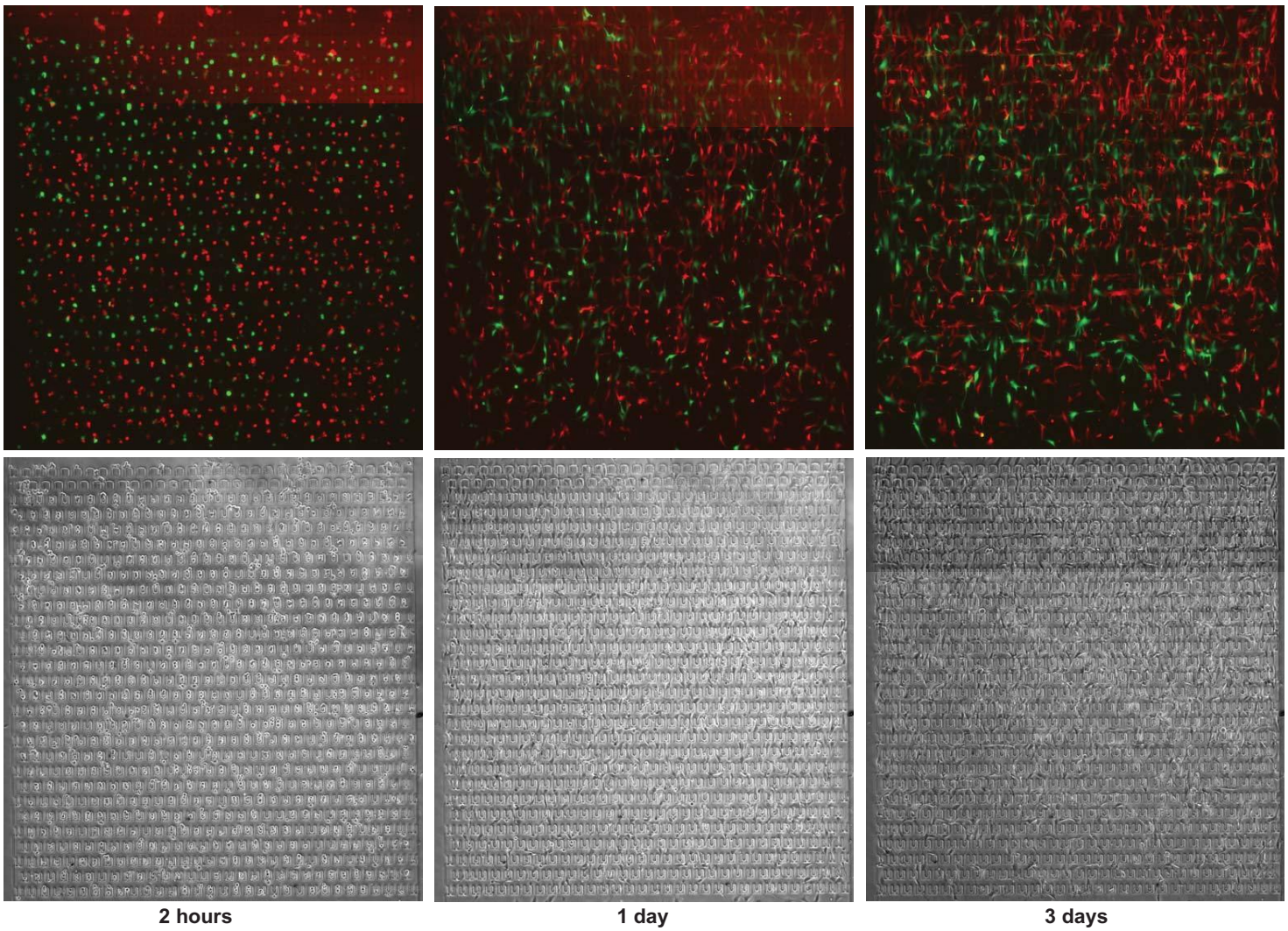

Fluorescence and phase images of 3T3 cells loaded into a device and then cultured for 3 days in the absence of fusogenic stimulus, and imaged at 2 hrs, 1 day, and 3 days after loading. A mixture of red- and green-labeled cells were introduced into the device. No doubly labeled cells are apparent even three days after introduction into the device, suggesting that fusion in the absence of stimulus is negligible. The results also demonstrate the ability to culture cells for extended periods in the device.

Supplementary Figure 8

Fusion in the large array

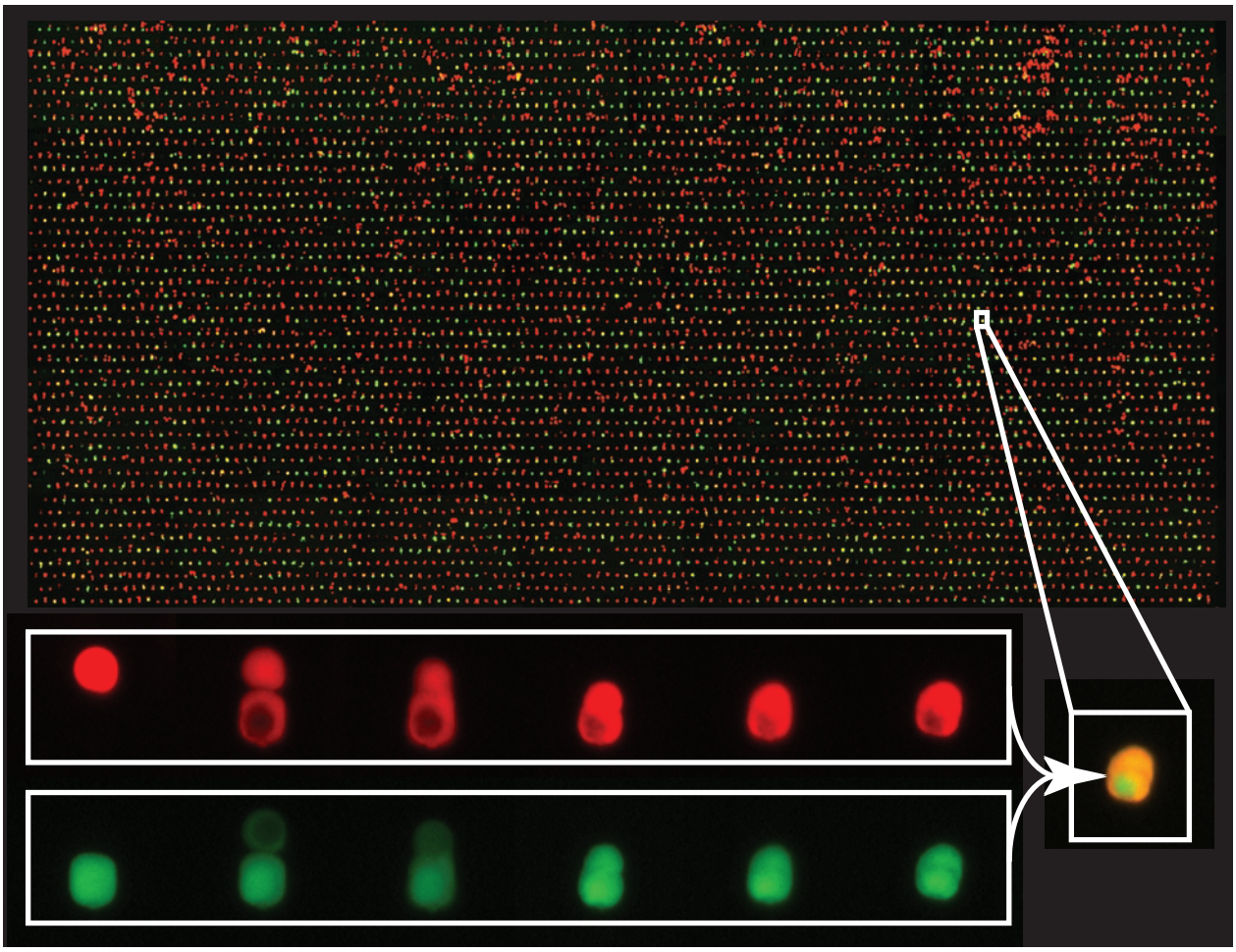

Red/green fluorescent overlay images of DSRed/eGFP cells fused in the 8 x 4mm array. The timescale of fusion in this large device was identical to that observed in the 2 x 2mm device. The image was taken at t = 25 min, and it is a composite of many images to cover the large array in sufficient detail.

Supplementary Figure 9

Analysis of fusion over time in CellTracker-stained cells

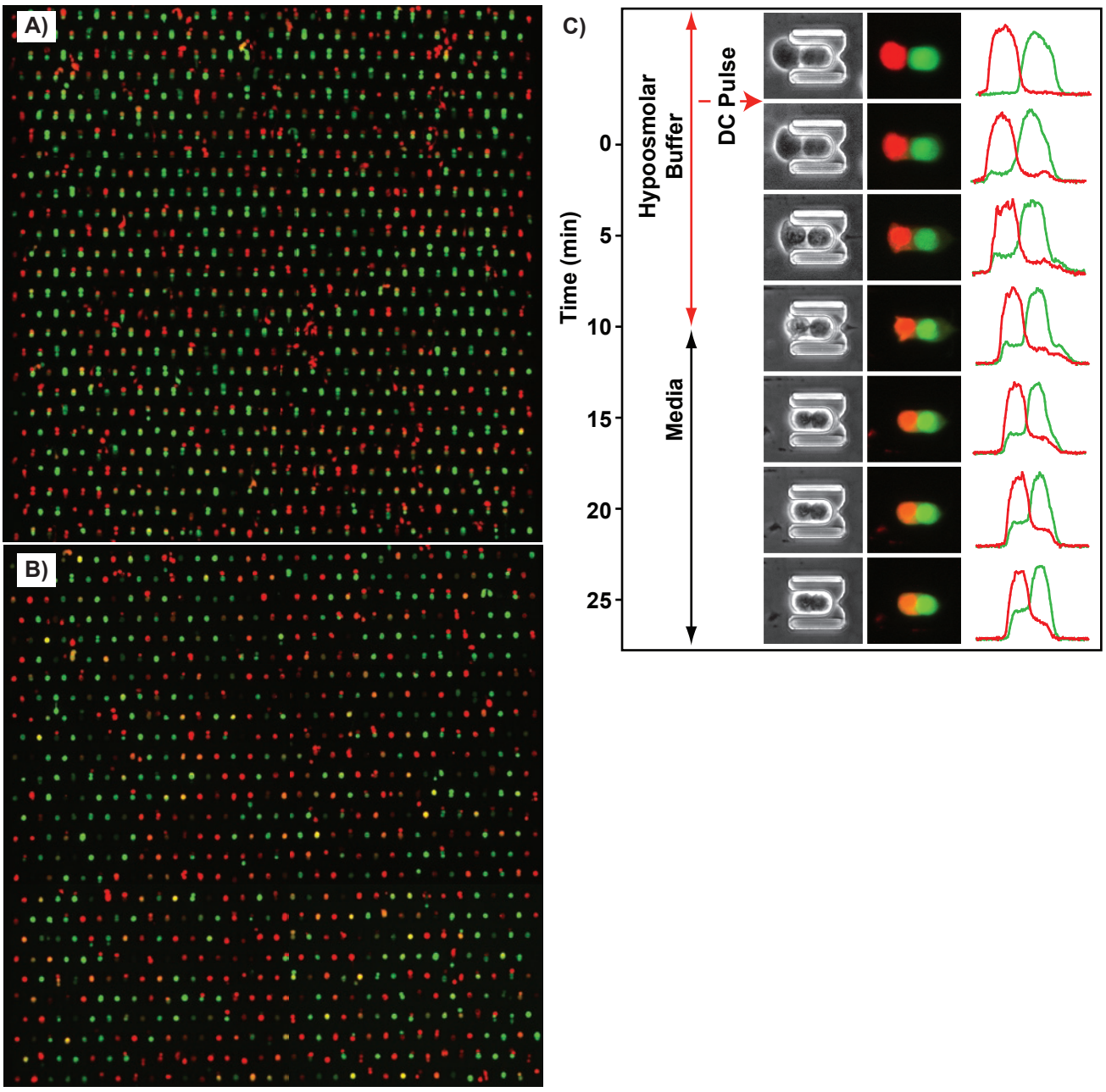

Red/green fluorescent overlay images of CellTracker stained 3T3s (A) and DSRed/EGFP 3T3s fused in the 2 x 2mm device. Both images are at t=25 min. Note that in (A) while the cells have exchanged fluorescence the majority of them still appear to be distinct, while in (B) the majority of the cells have reorganized into one hybrid cell. These cells were fused on the same day under identical electrofusion conditions. (C) Timescale of electrofusion of CellTracker stained 3T3s. Low level fluorescence exchange is observed immediately after the fusion pulse, and membrane reorganization is observed at t=15 min, similar to the timescale of DSRed/EGFP fusion is Figure 3. However, at t=25 min the fluorescence is still segregated even though one cell membrane is observed.

Supplementary Figure 10

Schematics of photomasks used to fabricate device

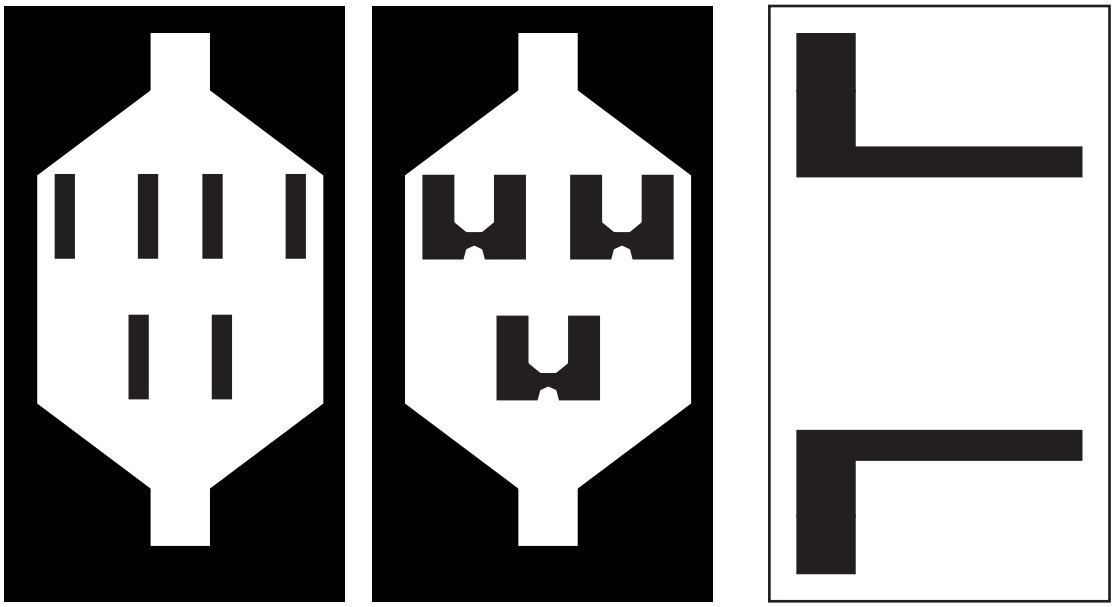

Capture device mask 1 **Capture device mask 2** **Electrode mask**

Schematics of photomasks used to fabricate the PDMS device and electrodes. The first layer darkfield photomask contains the outline of the channels and the support pillars, and the second layer mask contains the outline of the channel and the detail of the trap. The electrode mask is a lightfield mask.

Supplementary Methods

1. Details of microfabrication

The first layer of photoresist (SU-8 2007, MicroChem, Newton, MA) was spun at 2500-3000 rpm for 30 s, yielding feature heights of 6 to 8 μm. The wafers were exposed to UV light through a chrome photomask (**Supplementary Fig. 10**, Advance Reproductions, North Andover, MA) using a contact aligner (Karl Suss, Waterbury, VT). After developing and baking, the second layer of SU8 (SU-8 2015, MicroChem) was spun at 3500 rpm for 30 s, yielding features heights of 12-14 μm. Overall feature heights of 18 to 24 μm were obtained. The SU-8 molds were silanized for 24 hr in a vacuum chamber saturated with (tridecafluoro-1,2,2-tetrahydrooctyl)-1-tricholorosilane (T2492-KG, United Chemical Technologies, PA).

PDMS (Sylgard 184, Dow Corning, MI) was poured over the master and then degassed for ~1 hr before curing at 65 ^{o}C for ~4 hrs. After curing, thin walled stainless steel tubing (0.07"ODx0.0653"ID, Small Parts Inc.) was used to puncture reservoirs.

Glass slides with electrodes were constructed from mask blanks pre-coated with chrome and photoresist (Telic, Valencia, CA), The mask blanks were exposed through a transparency mask (PageWorks, Cambridge, MA), and then developed in NaOH. After etching, the remaining photoresist was removed using acetone. Wires were bonded to the chrome electrode pads using conductive epoxy (Circuit Specialists, Mesa, AZ).

The PDMS devices and glass slides were oxygen plasma cleaned (PDC-001, Harrick Scientific, Ossining, NY) for 1 min prior to bonding. The devices were aligned to the glass and/or electrodes, lightly pressed together and then left to bond at 65^{o}C for 30 min.

2. Device setup

The microfluidic device was first filled with 70 % ethanol then PBS. The surface of the device was blocked using 7.5% BSA and incubating at room temperature for 1 hr. The device was rinsed with PBS before assembling. PEEK tubing connected to a 4-way valve (UpChurch Scientific, WA) was plugged into the bottom outlet of the device. This valve was also connected to a manual syringe and a glass syringe on a syringe pump. Cells and fusion buffers were pipetted directly into the top inlet reservoir and drawn

through the device at flow rates of 0.4-0.6 μL/min, corresponding to ~ 15-50 μm/s. Devices could be reused for 2-3 rounds of fusion as long as cells were removed prior to attachment.

3. Cell culture and staining

NIH3T3 mouse fibroblasts were purchased from ATCC and cultured in media containing Dulbecco's Modified Eagle's Medium (DMEM) supplemented with 10% bovine calf serum, 4 mM L-glutamine, 100 U/mL penicillin, and 100 μg/mL streptomycin . Cells were typically passaged 2 days before experiments and used when almost confluent. NS-1, a non-secreting myeloma cell line, was maintained in DMEM.

V6.5 mESCs were cultured on irradiated primary embryonic fibroblasts and used for experiments after depletion of feeder cells by preplating. mEFs were derived from E14.5dpc Balb/c mice. Where indicated, ES cells, mEFs and B cells were used expressing CAGGS-GFP from the Rosa26 locus (clone HS2.1, manuscript in preparation). mEFs were generated from mice carrying an Oct4-GFP reporter in their endogenous locus[27]. Drug selection was performed using Hygromycin B (125 μg/mL) and Puromycin (2 μg/mL). Reprogrammed cells were cultured on mEFs. The media used after all fusion protocols was prepared as above but with phenol red-free DMEM.

3T3s and mEFs were washed with PBS and incubated with stain in serum-free media (CellTracker Green CMFDA: 1.25 μg/mL; CellTracker Orange CMTMR: 2.5 μg/mL; Hoechst 33342: 5 μg/ml; all dyes originally dissolved in DMSO) for 30 min. The cells were again washed with PBS, then incubated in regular media. The cells were typically stained 3 hours or more before experiments. ES cells were stained in suspension to enable even dye uptake. The cells were first dissociated, spun down, resuspended in stain and incubated at 37 ^{o}C for 5 min, then spun down and resuspended in media for 15 min.

Staining for alkaline phosphatase was done according to the manufacturer's protocol (Vector Laboratories).

4. Voltage Optimization

Device: The conditions for fusion were optimized in our four channel device. The device was bonded to a glass slide with electrodes whose gaps varied but were connected to one contact pad (**Fig. 1, Supplementary Fig. 3**). Simultaneous testing of four different electric fields was possible with the application of a single voltage pulse. Electric fields for fusion of 3T3 cells were evaluated on the basis of membrane reorganization. Optimal field strength was determined to be 0.63 kV/cm, and this field strength was also used for fusion of mESCs/mEFSs and B-cell/myelomas.

Controls: Optimal fields were decided on the basis of best fluorescence exchange (highest percentage of red+green cells). 3T3 cells stained with CellTracker were subjected to different fusion voltages in triplicate and analyzed by FACS. Optimal field strength was determined to be 1.0 kV/cm, and this field strength was used for all cells fused in the Helix chamber.

Standard PEG Fusion: $5x10^5$ cells of each cell type were pelleted and kept at 37 ^oC during the fusion protocol. PEG-fusion was performed according to the manufacturer's protocol (Roche Applied Science, Mannheim, Germany). Briefly, 100 μL of PEG 1500 was added over 3 min while stirring gently with the pipet tip and pre-warmed media was then added. The cells were then pelleted, resuspended in 900 μL of media, and incubated for the remainder of 25 minutes. At t=25 min, the cells were fixed by adding 100 μL of 10% formalin and analyzed using a FACS LSR II (Becton Dickinson, San Jose, CA).

Commercial electrofusion: $5x10^5$ cells of each cell type were pelleted and resuspended in 250 μL of hypoosmolar fusion buffer (Eppendorf, Westbury, NY) and transferred to the fusion chamber (Helix fusion chamber, Eppendorf). The cells were aligned before and after the pulse by applying 6V AC for 60 s, and pulsed at varying voltages (0.5 to 2.0 kV/cm) for 50 μs x 5 pulses. After 10 min the cells were washed from the chamber into media, and incubated at 37 ^oC. At t=25 min the cells were fixed and analyzed as above.

5. Image Acquisition and Analysis

The microfluidic device was placed on an automated inverted microscope (Zeiss Axiovert 200m, Zeiss, Thornwood, NY) fitted with a stage incubator (In Vivo Scientific, St. Louis, MO). During the entire fusion protocol the device remained in place and images were acquired on a Spot camera (Spot RT Color 2.2.1, Spot Diagnostic, Sterling Heights, MI) using MetaMorph (Molecular Devices, Sunnyvale, CA). Images were taken either every 2.5 min or 5 min, and at each time point phase and fluorescent images were acquired.

Images were analyzed in ImageJ (http://rsb.info.nih.gov/ij/). Any scaling of intensities for visualization was applied uniformly to the entire series of images from an experiment. Pairing efficiencies were calculated by determining the number of traps in the field of view and those occupied with a single cell of one type in the bottom of the well with a second cell (or more) of the other type on top. Only cells in contact and paired within the capture cup were considered. Fusion efficiencies were determined by observing each set of paired cells over the time series.

Fluorescence exchange efficiencies were also analyzed using an automated macro written in ImageJ . An array tool placed small boxes at the base and top of each capture cup within the image (**Supplementary Fig. 4**). Red and green fluorescent images were treated separately, and then the mean green and red values were plotted for each box, resembling a FACS plot (**Supplementary Fig. 6**). Each timepoint was treated separately while keeping the box locations the same. The mean green and red intensities from the entire set of images were then scaled between 0-1023, converted to an .fcs file using a2fcs.exe (http://www.umass.edu/microbio/mfi/verifhlp/verifyfc.htm) and analyzed in FlowJo. The data from before the pulse was used to determine the location of the red-green-positive gate, and this gate was applied to the rest of the data sets within the series. The fusion efficiencies were represented by the number of red-green double-positive cells over the total number of cells (number of red-green double-positive boxes over total number of boxes).

For the quantitation in **Fig. 4**, each data point represents one image field over a single run, and data was obtained from 3 different runs with different cells loaded freshly into the device each time.

Supplementary Discussion

Device and protocol optimization for other cell types

Cells of different sizes: The geometries used here were optimized for cell types of similar size, such as mEFs and mESCs; pairing of cell types that are significantly mismatched or different than these cells (~15 μm) requires re-optimization of the cup and gap dimensions. As a starting point for optimization, the single-cell cup should be sized to trap the smaller cell, sizing the vertical gap small enough to prevent the cell from squeezing through the gap. The two-cell cup should then be sized for the combination of the smaller and larger cell.

Optimizing fusion protocols: Optimization of cell fusion in the device is substantially the same as occurs with standard PEG or electrofusion protocols, with some added advantages due to the format of the device. Specifically, because we can observe cells following the fusion pulse but before removal from the device, optimization is faster than in conventional approaches. In addition, because cell pairs all see the same environment, our results suggest less run-to-run variability in the device than in conventional approaches (e.g., ~60% variability for Celltracker-stained fibroblasts in the device vs. ~150% variability in conventional approach, **Fig. 4(b**)).

For PEG fusion, we used the standard bulk protocol but added multiple PEG doses, with fusion efficiency increasing with dose number, limited by the fact that cell death increased with dose as well (**Supplementary Fig. 2**). We did alter PEG exposure time and the transition time going back from PEG to media, but did not find significant changes in performance except in extreme conditions (e.g., very long PEG exposures, which decreased viability). For electrofusion, we used standard electrofusion buffer and a special optimization device containing arrays of chambers with differently spaced electrodes, allowing exposure of identical cell populations (same culture, feeding conditions, etc.) to distinct electric fields at once (**Supplementary Fig. 3**), which is impossible to do with conventional approaches. One significant change between conventional and microfluidic electrofusion is that the pre-fusion dielectrophoretic force applied in conventional approaches is unnecessary in the microfluidic device. As with

conventional electrofusion, optimization occurs by finding the voltage that starts to cause significant cell death and then reducing the field slightly.

Once a fusion protocol was found, we found the results to be consistent across runs (**Fig. 4**), with variations in the health of the cell population before fusion being most critical, as with conventional approaches. Thus, obtaining cells in log phase, recently fed, recently trypsinized, and kept warm, tends to increase fusion efficiency.

Given the unique format of the microfluidic device, there are opportunities in using fusion protocols more widely distinct from conventional approaches, such as using hydrodynamic forces to alter local membrane curvature of the fusing cells, altering the PEG fusion sequence, combining PEG with electrofusion, etc.